SSBI counteraction technology in a single photodetector-based direct detection system receiving an independent dual-single sideband signal

ZHENG HU, JIANGNAN XIAO,* YILIN CHEN, JIABAO ZHAO, FEIHAN LI, AND HANGZHI ZHU

University of Shanghai for Science and Technology, Shanghai 200093, China
jiangnanxiao@usst.edu.cn

Abstract: To further meet the large capacity, high spectrum efficiency (SE), reduce the signal-signal beat interference (SSBI) of the independent dual single sideband (ISB) system and the complexity of the receiver, we propose an iterative signal-signal beat interference counteraction (ISSBIC) algorithm to suppress SSBI. The 16-Gbps left sideband and the 16-Gbps right sideband signals in the ISB system are quadrature phase-shift keying (QPSK) modulated. After standard single-mode fiber (SSMF) transmission, the LSB and RSB signals are synthesized to a 16-quadrature amplitude modulation (QAM) signal after conversion through the photodetector (PD) square law. The simulation results show that the ISSBIC with just 2 iterations is superior to Kramers–Kronig (KK) receiver in processing the system error bit. In the meantime, the ISSBIC requires a sampling rate of 20GSa/s, whereas KK requires 40GSa/s. Moreover, the proposed ISSBIC algorithm has a simpler complexity. According to the simulation results, the suggested ISSBIC receiver can lower the ADC requirements and system costs, which opens up a wide range of applications in multiplex and higher SE transmission systems.

1. Introduction

In recent years, demand for mobile communications capacity is rising rapidly, driven by emerging broadband applications such as cloud computing, the Internet of things and augmented/virtual reality [1–4]. People usually have higher requirements on the transmission rate and system bandwidth of optical communication. A lot of work has been devoted to the development of advanced optical communication receivers to improve the performance of optical fiber communication. Compared with coherent reception [5–7], direct detection (DD) is widely favored due to its low cost and flexibility. Research on optical independent sideband (O-ISB) modulation has been quite active recently. Because single sideband (SSB) modulation only uses one side band for information transmission, spectrum resources are wasted [8,9]. Device costs are certainly raised by the requirement for two optical bandpass filters (OBPFs) and two photodetectors (PDs) in the classic independent dual SSB system [10]. By transferring distinct data over the left and right side bands, O-ISB modulation significantly increases spectrum efficiency (SE) while avoiding the aforementioned drawbacks. In addition, a straightforward digital signal processing (DSP) is used at the receiver end to store the signal rather than two sharp, narrow OBPFs.

Nevertheless, because of the photodetector's beat effect at the receiving end, signal-to-signal beat interference (SSBI) poses a significant challenge in the system mentioned above [11–13]. To suppress SSBI, many schemes have been proposed. A carrier-suppressed single sideband transmission scheme is proposed to reduce the impact of beat interference by inserting a frequency interval, but this scheme can sacrificed SE [14]. There have been several demonstrations that

Kramers Kronig (KK) receiver is an effective scheme [15–19]. In [16], KK algorithm was introduced into the receiver, which effectively mitigated SSBI under the minimum phase condition, but there were certain requirements for carrier power in this design. In [19], the first all-analog KK signal processor has been proven suitable for SSB DD optical communication systems again. The results have shown that it can reduce the symbol error rate of a 16QAM system running at 500Mbit/s by at least a factor ten. Another attractive approach is to use an iterative form to remove crosstalk [20–22]. In [20], an iterative elimination algorithm was used to slow down the receiving scheme of SSBI while improving SE, but the number of iterations in this scheme may increase the complexity of the receiver. In [21], the concept of iterative linear equalizer based on first-order linear equalizer was proposed. In short, it is to make repeated use of first-order linear equalizer to achieve better SSBI mitigation effect, but the complexity of receiver DSP algorithm is increased due to the introduction of multiple iterative operations. The problem is similar to [20].

In the study, we successfully implement an ISB system based on a low complexity receiver. At the transmitter end, the left sideband (LSB) 4QAM and right sideband (RSB) 4QAM signals simultaneously carry individual data and add a virtual carrier (VC) on one side of each side band. At the receiver end, a single PD is used to receive the signal and separate the left sideband (LSB) and right sideband (RSB) signals by DSP in the electrical domain. In addition, the scheme effectively eases the resolution requirement for the DAC on the transmitting side because the higher-order QAM signal is synthesized by first generating the low-order QAM sideband signal in the electrical domain and then mixing it with PD, as opposed to generating and transmitting the higher-order QAM signal directly.

The remainder of this article is organized as follows. The relevant principles are described in Section 2. The simulation setup for the ISB system is described in Section 3 The simulation results are analyzed in Section 4. Section 5 concludes the article.

2. Principle

2.1. ISB DD with virtual carrier

At the transmitter end, the radio frequency (RF) signal consists of a modulated HF signal and a VC. At the receiver end, the LSB, RSB signals and the corresponding VC beat each other at the PD generating the intermediate frequency (IF) signal. The IF signal is easy to be overlapped with SSBI, which interferes with the demodulation of the signal. Figure 1 illustrates the principle of photonic frequency down conversion. A VC is added to each side of a pair of HF signals with bandwidth B respectively. The frequency interval between the VC and the HF signal can be adjusted arbitrarily. Then the HF signal and the added VC beat each other at the PD to complete the down-conversion.
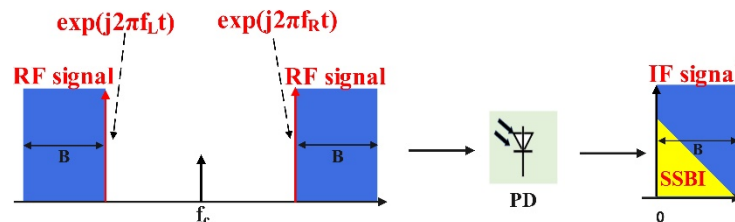

Fig. 1. Spectrum of ISB signal before and after PD square-law detection based on photonic frequency down-conversion. Here, f_L and f_R are virtual carriers.

Since the square law of PD causes SSBI to be created during the conversion process. If the frequency interval is less than 1.5B, the converted IF signal frequency will overlap with

SSBI partly. If the frequency interval is 0 GHz, the converted signal the converted signal will completely overlap with the SSBI. When the frequency interval exceeds 1.5B, the received IF signal frequency after down-conversion remains quite high, which can have a significant impact on the cost of receiver. Therefore, the frequency interval should be narrowed between the VC and the HF signal as much as possible. The ISSBIC algorithm is mainly considered in our scheme.

2.2. Principle of the proposed scheme

Figure 2 depicts the process of SSBI reconstruction and elimination by ISSBIC and KK algorithms.
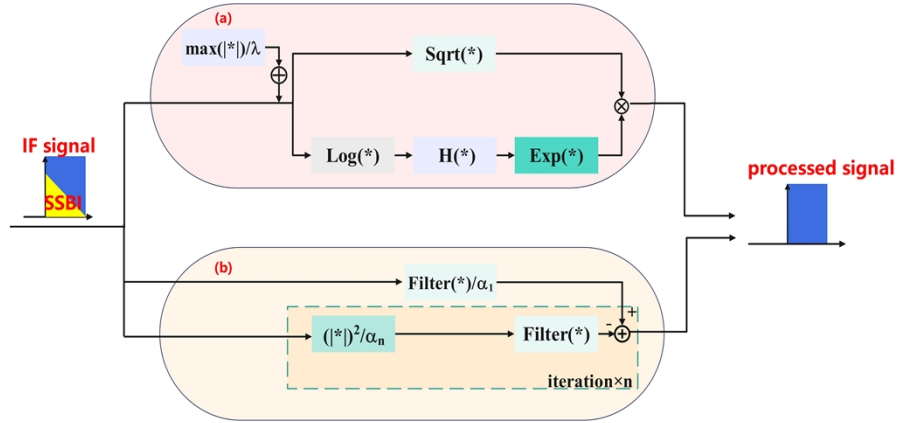
Fig. 2. Block diagram of SSBI suppression algorithm. (a) the KK scheme. (b) the ISSBIC scheme. H(*) represents a Hilbert transform. $|*|$ stands for absolute value. Filter(*) represents a single sideband filter. α and λ represent the ratio factor.

It is evident from Fig. 2(a) that the KK relation describes the phase reconstruction and can be used to recover the signal's phase from its intensity. To further improve the preformance, direct current (DC) can be added during the reconstruction step to remove the phase jump inaccuracy.

Figure 2(b) shows the ISSBIC scheme, the core concept is to save the intensity information of received signal, iteratively reconstruct and cancel SSBI using a single sideband filter and varying rating factors after each iteration.

First, the photocurrent after PD is divided into two channels. One signal is allowed to pass through a single side band filter and its amplitude is controlled by a rating factor, as shown in Eq. (1).

$$S(t) = F(I(t))/\alpha_1 \tag{1}$$

where I(t) is the photocurrent after PD injection, F(*) and α_1 represent a single sideband filter and the rating factor of the first iteration respectively.

The first SSBI estimation is obtained from another signal, as shown in Eq. (2).

$$SSBI_1 = F[\text{abs}(I(t))^2/\alpha_1] \tag{2}$$

The second SSBI estimation is obtained from another signal, as shown in Eq. (3).

$$SSBI_2 = F[\text{abs}(S(t) - SSBI_1)^2/\alpha_2] \tag{3}$$

where α_2 represents the rating factor of the second iteration.

Therefore, it is not difficult to obtain the nth SSBI estimation, as shown in Eq. (4).

$$SSBI_n = F[\text{abs}(S(t) - SSBI_{n-1})^2/\alpha_n] \tag{4}$$

where the number of iterations is less than 1, the SSBI value is set to 0, α_n respresents the rating factor of the n_{th} iteration. As the number of iterations tends to infinity, $SSBI_n$ tends to SSBI.

Finally, SSBI is subtracted from the signal after PD to eliminate crosstalk, where the value of the ratio factor is re-selected after each iteration to approximate the SSBI.

2.3. Principle of the ISB signal generation

Figure 3 illustrates the principle of the ISB system. Here, (I), (II), (III), (IV), (V) represent the spectrogram of the RSB signal, the LSB signal, the modulated independent dual-SSB signal, the modulated independent dual-SSB signal after I/Q modulation and the received signal after PD, respectively. First, at the transmitter end, two independent pseudo-random binary sequences (PRBSs) are mapped by QPSK, upsampled and root raised cosine (RRC) filtered to generate LSB and RSB signals. Then, the generated signals are up-converted to RF signals by mixing with two carriers that are in the complex sinusoidal form: $\exp(-2\pi f_s t)$ and $\exp(2\pi f_s t)$. The LSB and RSB signals can be expressed as follows:

$$E_L(t) = \exp[j\psi_L(t)] \exp[-j\omega_s(t)] \tag{5}$$

$$E_R(t) = \exp[j\psi_R(t)] \exp[j\omega_s(t)] \tag{6}$$

where $\psi_L(t)$ and $\psi_R(t)$ denote the phase of the LSB and the RSB signals respectively. Here, $\omega_s(t) = 2\pi f_s(t)$, R > 0, R = -L. Then, virtual carriers (VCs) are added to the LSB and the RSB signals respectively. Therefore, the LSB and the RSB signals after the VCs are added can be expressed as follows:

$$E_L(t) = \exp[j\psi_L(t)] \exp[-j\omega_s(t)] + \exp(j\Phi_L(t)) \tag{7}$$

$$E_R(t) = \exp[j\psi_R(t)] \exp[j\omega_s(t)] + \exp(j\Phi_R(t)) \tag{8}$$

$$E(t) = E_L(t) + E_R(t) \tag{9}$$

where $\Phi_L(t) = 2\pi f_L(t)$, $\Phi_R(t) = 2\pi f_R(t)$, $\Phi_L(t) = -\Phi_R(t)$ Here, Eq. (9) describes the drive signal of the I/Q modulator. The output signal through the I/Q modulator can be written as:

$$\begin{aligned} E_{IQM}(t) &\approx E_{CW}(t)\{J_{-1}(\alpha)[\exp(-j\omega_s(t) + j\psi_L(t)) \\ &+ \exp(j\Phi_L(t)] + J_1(\alpha)[\exp(j\omega_s(t) + j\psi_R(t)) \\ &+ \exp(j\Phi_R(t))]\} \end{aligned} \tag{10}$$

where $J_{-1}(\alpha)$ and $J_1(\alpha)$ are Bessel function of the first class, α is the modulation coefficient. Then the output signal is directly fed into the PD. Assuming that a low bandwidth PD is used, the high-order terms generated from the cross-beating between the LSB and RSB signals can be removed. The DC component can be filtered. Therefore, the simplified photocurrent can be expressed as:

$$\begin{aligned} i(t) &\approx R \cdot J_{-1}^2(\alpha)\{\cos((\omega_s + \Phi_L)t - \psi_L(t) + \\ &\cos((\omega_s - \Phi_R)t) + \psi_R(t)) - 2\cos(\psi_L(t) + \psi_R(t)) \end{aligned} \tag{11}$$

where R is the PD responsivity. Here, the first two terms are the desired signal and the third term is SSBI which can be suppressed by ISSBIC or KK in Eq. (11).

2.4. Principle of the synthesized 16QAM signal

One constellation point of LSB signal and one constellation point of RSB signal can completely modulate each constellation point of 16QAM signal, as shown in Fig. 4. The mapping relationship between the transmitted and received signals is indicated by the colors and positions of the synthesized points in the various constellations. For example, the test constellation point in the diagram is a superposition of a blue constellation point for symbol 0 in the LSB and a red constellation point for symbol 2 in the RSB.
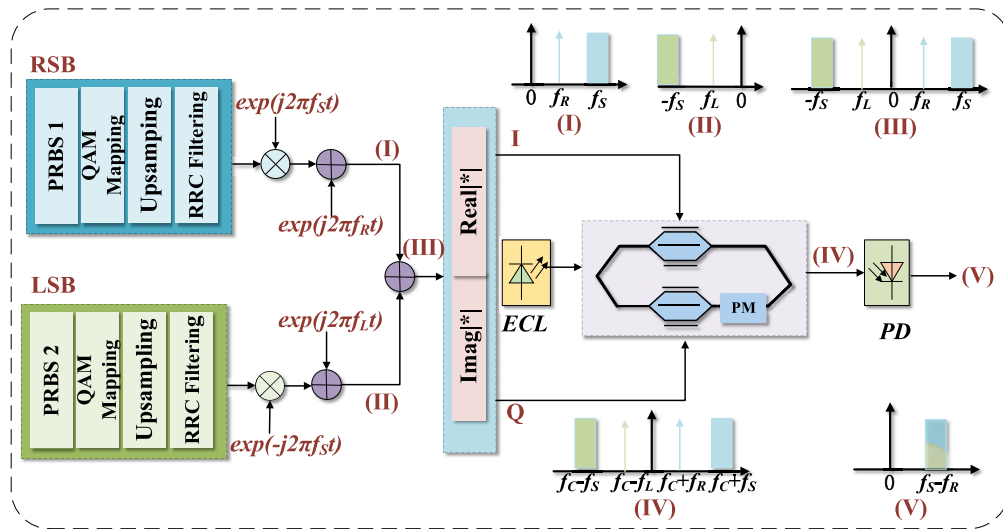
Fig. 3. Scheme of the ISB signal generation. (I) The electric spectra of the RSB signal. (II) The electric spectra of the LSB signal. (III) The electric spectra of the ISB signal. (IV) The optical spectra of the signal after IQ Mod. (V) The electric spectra of the received synthesized signal after PD.
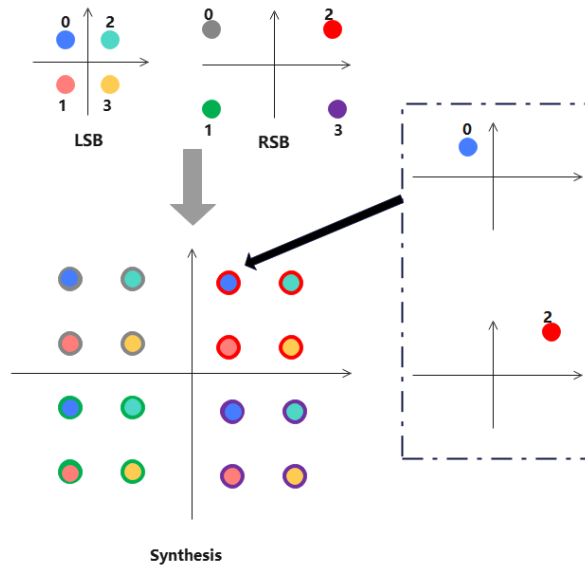

**Fig. 4.** Schematic diagram of 16QAM signal synthesis.

3. Simulation setup

The simulation setup of proposed scheme is shown in Fig. 5. To verify the proposed scheme, corresponding simulation experiments were carried out to generate a 16QAM signal from two 8-Gbaud independent dual ssb QPSK signals, and the receiving PD directly detected the reception based on frequency conversion and ISSBIC algorithm.

At the transmitter end, two independent bit sequences are generated by the random number generator. QPSK modulation is performed on the two data channels respectively, and the relative
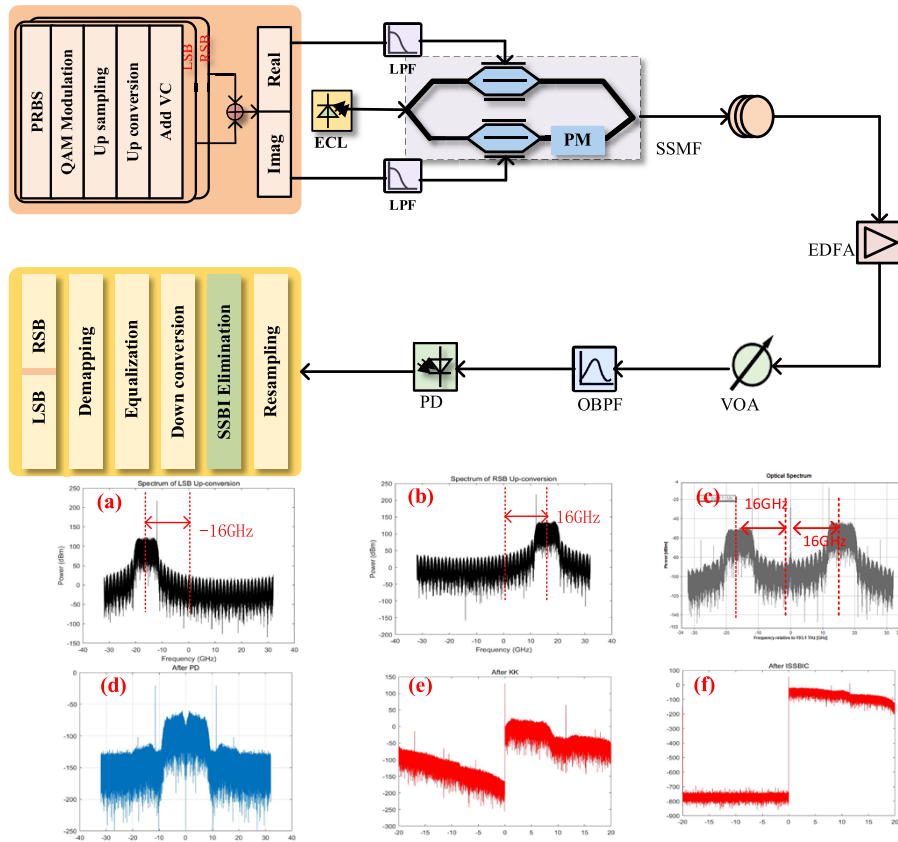
Fig. 5. Simulation system diagram. LPF: low pass filter; SSMF: standard single-mode fiber; EDFA: Erbium-doped fiber amplifier; VOA: Variable optical attenuator; PD: photodiode; (a) Spectrum of RSB Up-conversion; (b) Spectrum of LSB Up-conversion; (c) the output singal spectrum of I/Q MOD; (d) the electric spectra of the received signal with 0.5 GHz frequency interval after PD; (e) the electric spectra of the received signal with 40GSa/s and 0.5 GHz frequency interval after KK; (f) the electric spectra of the received signal with 40GSa/s and 0.5 GHz frequency interval after ISSBIC.
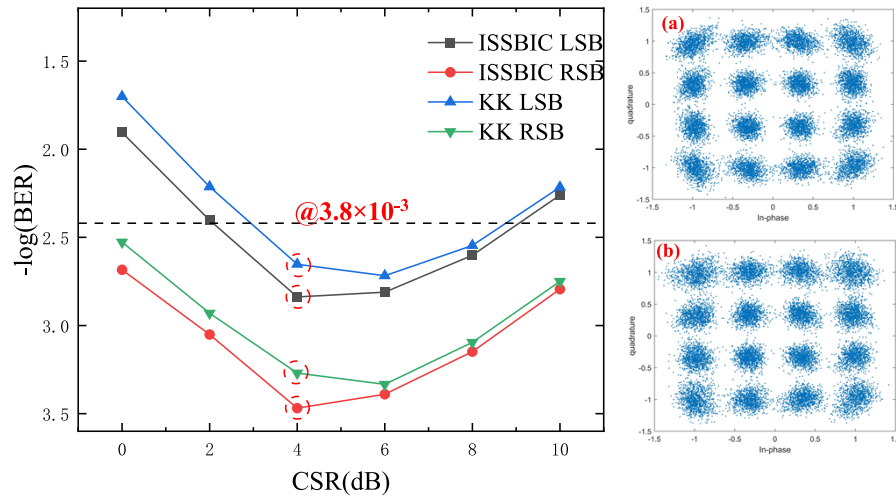
Fig. 6. BERs with ISSBIC and KK as a function of the CSR after 90 km SSMF. (a) Constellation diagram with ISSBIC when CSR is 4 dB. (b) Constellation diagram with KK when CSR is 4 dB.

power is adjusted. Then upsampling (64GSa/s) is performed, and the two baseband signals are shaped by the pulse of RRC filter roll-off factor of 0.1 at a bit rate of 16Gbps. Next, the baseband signals are converted to the desired LSB and RSB bands at -16 GHz and $+16$ GHz respectively. VCs are added to one side of the LSB and RSB respectively. The left and right side band HF signals and VCs are added to form the RF signal. The RF signal is divided into real and imaginary components. The I and Q branches of the I/Q modulator are driven by an electrical amplifier (EA) and a low-pass filter (LPF bandwidth < 20 GHz). An external cavity laser with a linewidth of 100KHz and optical power of 16dBm is used, and the emission frequence of the laser is 193.1THz. The half-wave voltage of I/Q modulator is set to 2.5 Volts. The I/Q modulate works at the lowest bias point.

After 90 km SSMF transmission, Erbium-doped fiber amplifier (EDFA), variable optical attenuator (VOA) are uesd to compensate optical power loss of transmission link and adjust the input optical power respectively. Then OBPF (bandwidth < 35 GHz) is used to constrain the bandwidth of optical signal before it is transmitted into PD. At the receiver end, the received signal is first resampled. Next, ISSBIC and KK algorithms are used to suppress SSBI respectively. After SSBI is eliminated, down-conversion, down-sampling, retiming, cascading multimode algorithm (CMMA), blind phase search (BPS) are performed on the signal, and then the LSB and RSB signals are separated from the 16QAM signal. Finally, the BER of the two sidebands is calculated.

4. Simulation results

Initially, we tested the relationship between the VC to HF signal power ratio (CSR) and BER. We set the frequency interval to 0 GHz, which indicates that the VC is particularly close to the signal bandwidth. This lowers the frequency of the low-IF signal following PD. The input optical power of PD is fixed at -13dBm. The number of iterations of ISSBIC is set to 2.

The OSNR and signal rate are set to 40 dB and 8-Gbaud. The resampling rate of the receiver end before being processed by KK and ISSBIC algorithm is set to 40GSa/s and 20GSa/s respectively. We keep the HF signal power constant and adjust the CSR by changing the VC power. The measured BER curve is shown in the Fig. 6. It is evident that when the CSR increases, the BER
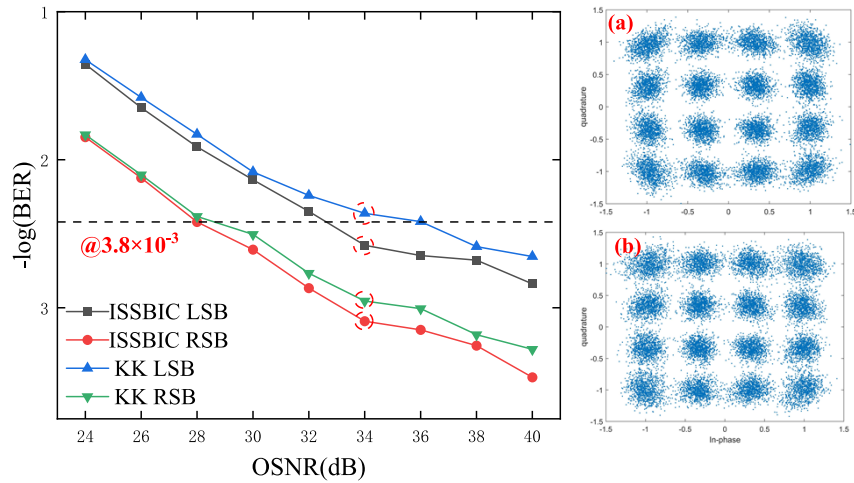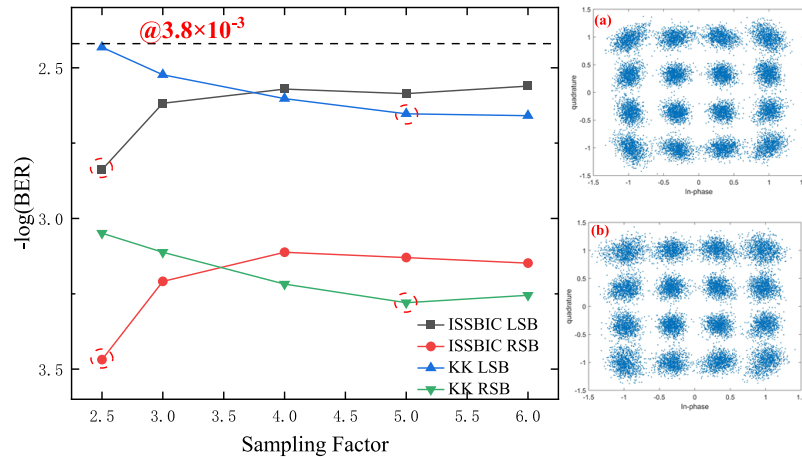
Fig. 7. BERs with ISSBIC and KK as a function of the OSNR after 90 km SSMF. (a) Constellation diagram with ISSBIC when OSNR is 34 dB. (b) Constellation diagram with KK when OSNR is 34 dB.
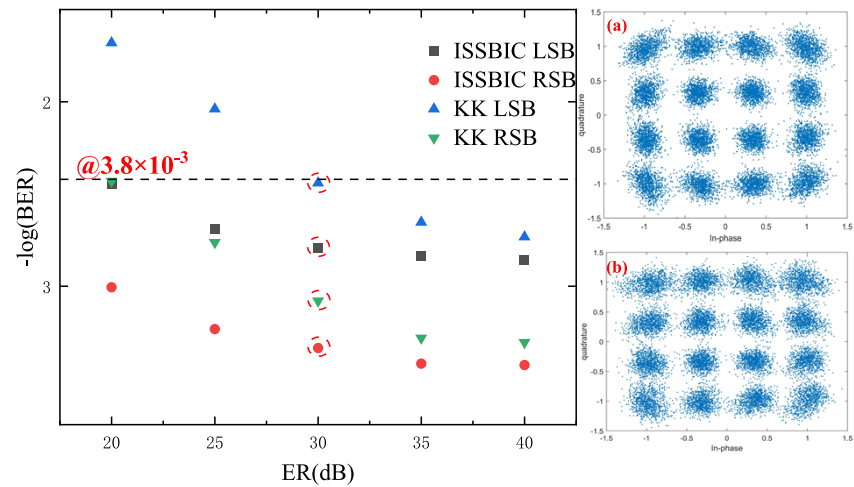
Fig. 8. BERs with ISSBIC and KK as a function of the ER after 90 km SSMF. (a) Constellation diagram with ISSBIC when ER is 30 dB. (b) Constellation diagram with KK when ER is 30 dB.

of the LSB and RSB signals initially decreases and subsequently increases. It is evident that ISSBIC inhibits SSBI more effectively than the KK algorithm. Furthermore, 4 dB and 6 dB are the ideal CSR values for the ISSBIC and KK. It suggests that the KK algorithm needs more VC power, which translates to a higher system energy usage. In addition, the ISSBIC only requires two iterations.

Next, we measured the relationship between the OSNR and BER. The CSR is set to 4 dB and the other simulation conditions are the same as the previous one. It can be seen from the Fig. 7 that ISSBIC with 2 iterations requires a lower OSNR than KK (approximately 4 dB lower), and KK also has a greater sampling rate when the BER of both the LSB and RSB signal are below the threshold.
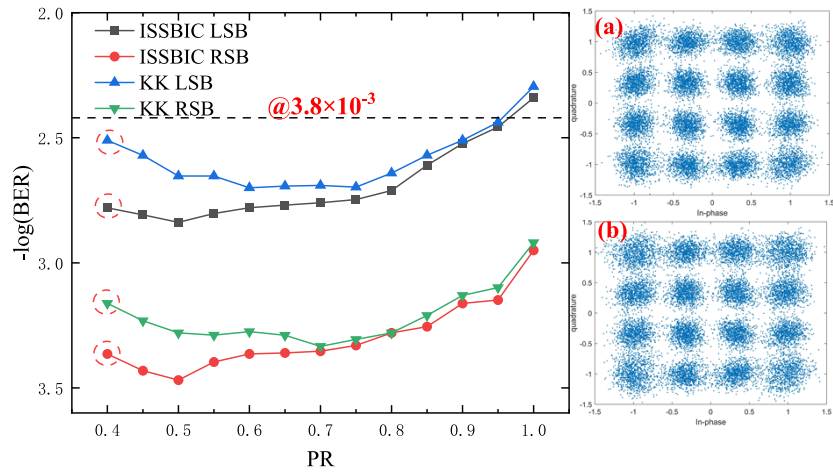
Fig. 9. BERs with ISSBIC and KK as a function of the Sampling Factor after 90 km SSMF. (a) Constellation diagram with ISSBIC when Sampling Factor is 2.5. (b) Constellation diagram with KK when Sampling Factor is 5.

Then we analyzed the effect of different ExtinctionRatio (ER) values on the BER. To better compare the two algorithms, the OSNR is fixed at 40 dB and other conditions remain unchanged. The impact of ER on the performances of KK and ISSBIC with 2 iterations is shown in Fig. 8. When ER is 20 dB and 30 dB, the BER of ISSBIC and KK can fall below the threshold respectively. Obviously KK requires a higher ER value than ISSBIC. Consequently, the latter has better robustness.

In the next stage, we evaluated the effect of different Sampling Factors on the BER. The BER curve trends of KK with regard to the sample rate and ISSBIC with two iterations are clearly different, as shown in Fig. 9. The BER of the KK algorithm steadily drops as the sampling factor rises. The best results are obtained when the sample rate is 40GSa/s (sampling factor is 5). The ISSBIC trend is reversed, with the best performance at a sampling rate of 20GSa/s (sampling factor is 2.5). In the case of two iterations, the sampling rate required for ISSBIC to achieve optimal performance is half of KK.

The relationship between the variation of RF signal power and the BER is depicted in Fig. 10. The power ratio (PR) represents the amplification factor of the power of the RF signal. From the general trend, the BER curves of ISSBIC and KK both decrease first and then increase with the increase of PR. The optimal PR values for ISSBIC and KK are 0.5 and 0.7 respectively, and obviously the RF signal power of ISSBIC is lower, which implies that it uses less power and is less expensive for the system.

The Fig. 11 shows the relationship between the received optical power (ROP) and the BER curve after the signal has been transmitted for 90 km SSMF. Since the average power of LSB signal is less than the average power of RSB signal, the anti-interference ability of LSB signal is weaker. Therefore, the BER of RSB signal is lower than LSB signal. With the increase of optical power, the BER gradually decreases. The BER performance of ISSBIC is lower than that of KK when the number of iterations is 1, particularly the BER of the LSB singal is consistently higher than the threshold. The BER of ISSBIC tends to be well as the number of iterations grows. In terms of performance, ISSBIC with 2 iterations beats KK and the sampling rate is lower. Due to the excessive number of iterations increasing the complexity of the system, and since the algorithm's performance has already met expectations after two iterations, we will not discuss cases with more than two iterations.

Fig. 10. BERs with ISSBIC and KK as a function of the PR after 90 km SSMF. (a) Constellation diagram with ISSBIC when PR is 0.4. (b) Constellation diagram with KK when PR is 0.4.
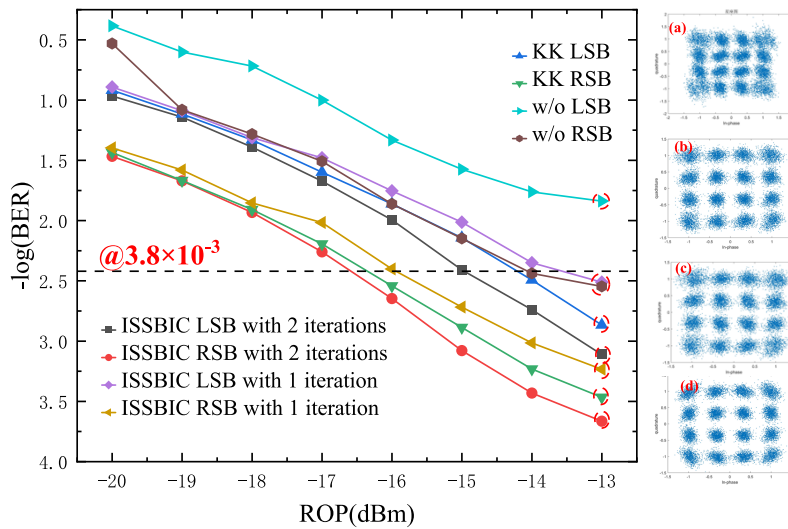
Fig. 11. BERs with ISSBIC and KK as a function of the ROP after 90 km SSMF. (a) Constellation diagram without ISSBIC and KK when ROP is −13dBm. (b) Constellation diagram with KK when ROP is −13dBm. (c) Constellation diagram with ISSBIC when ROP is −13dBm and the number of iterations is 1. (d) Constellation diagram with ISSBIC when ROP is −13dBm and the number of iterations is 2.

5. Conclusion

In this paper, a simple structure of ISB signal modulation and demodulation scheme is developed. In the aforementioned framework, a 8-Gbaud 16QAM signal is synthesized from two low-order signals via DD using a I/Q modulator. Concurrently, virtual carrier and signal carrier are used to strike each other in the PD to complete down-conversion technology before DSP to improve spectrum utilization. In DSP, SSBI is eliminated in DSP by employing an iterative approach before traditional equalization. The simulation results indicate that ISB tramission system with VCs employing ISSBIC technique performed well. ISSBIC with 2 iterations just needs half the sampling factor of KK technique to achieve optimal effect. In addition, the PR and ER values required by ISSBIC technique are also lower, so the system has well robustness. The transmission distance reaches 90 km SSMF, which basically meet the demand of short and medium-range optical communication. We believe this research has huge market prospects and application potential.

Disclosures. The authors declare no conflicts of interest.

Data availability. Data underlying the results presented in this paper are not publicly available at this time but may be obtained from the authors upon reasonable request.

References

1. J. Zhang, M. Lei, M. Zhu, *et al.*, "Optical-terahertz-optical seamless integration system for dual-λ 400 GbE real-time transmission at 290 GHz and 340 GHz," Sci. China Inf. Sci. **66**(11), 214301 (2023).
2. J. L. Wei, C. Sanchez, and E. Giacoumidis, "Fair comparison of complexity between a multi-band CAP and DMT for data center interconnects," Opt. Lett. **42**(19), 3860–3863 (2017).
3. Y. Pen, J. Huang, J. Luo, *et al.*, "Three-step one-way model in terahertz biomedical detection," PhotoniX **2**(1), 12 (2021).
4. X. Zang, B. Yao, L. Chen, *et al.*, "Metasurfaces for manipulating terahertz waves," Light: Adv. Manufact. **2**(2), 148 (2021).
5. W. Shieh, C. Sun, and H. Ji, "Carrier-assisted differential detection," Light: Sci. Appl. **9**(1), 18 (2020).
6. Y. Zhu, L. Li, Y. Fu, *et al.*, "Symmetric carrier assisted differential detection receiver with low-complexity signal-signal beating interference mitigation," Opt. Express **28**(13), 19008–19022 (2020).
7. P. Qin, C. Bai, Q. Qi, *et al.*, "Analytical Study and Noise Mitigation for Complex-Valued Optical DSB Transmission With Carrier-Assisted Differential Detection Receiver," IEEE Access **11**, 31443–31455 (2023).
8. T. Cho and K. Kim, "Effect of third-order intermodulation on radio-over-fiber systems by a dual-electrode MachZehnder modulator with ODSB and OSSB signals," J. Lightwave Technol. **24**(5), 2052–2058 (2006).
9. V. Sharma and S. Kumar, "Hybrid OFDM-OSSB-RoF transmission system incorporating fiber Bragg grating," Optik **124**(20), 4670–4672 (2013).
10. Y. Wang, J. Yu, H. Chien, *et al.*, "Transmission and Direct Detection of 300-Gbps DFT-S OFDM Signals Based on O-ISB Modulation with Joint Image-cancellation and Nonlinearity-mitigation," in *42nd European Conference on Optical Communication (ECOC)*, (IEEE, 2016), 1–3
11. S. Randel, D. Pilori, S. Chandrasekhar, *et al.*, "100-Gb/s discrete-multitone transmission over 80-km SSMF using single-sideband modulation with novel interference-cancellation scheme," in *2015 European Conference on Optical Communication (ECOC)*, (IEEE, 2015), 1–3
12. C. Sun, D. Che, H. Ji, *et al.*, "Study of Chromatic Dispersion Impacts on Kramers–Kronig and SSBI Iterative Cancellation Receiver," IEEE Photonics Technol. Lett. **31**(4), 303–306 (2019).
13. Z. Li, M. Erkilinc, K. Shi, *et al.*, "Digital Linearization of Direct-Detection Transceivers for Spectrally Efficient 100 Gb/s/λ WDM Metro Networking," J. Lightwave Technol. **36**(1), 27–36 (2018).
14. A. J. Lowery, L. Du, and J. Armstrong, "Orthogonal Frequency Division Multiplexing for Adaptive Dispersion Compensation in Long Haul WDM Systems," in *Optical Fiber Communication Conference and the National Fiber Optic Engineers Conference*, (IEEE, 2006), 1–3
15. A. Mecozzi, C. Antonelli, and M. Shtaif, "Kramers–Kronig coherent receiver," Optica **3**(11), 1220 (2016).
16. Y. Tong, Q. Zhang, X. Wu, *et al.*, "Integrated germanium-on-silicon Franz–Keldysh vector modulator used with a Kramers–Kronig receiver," Opt. Lett. **43**(18), 4333–4336 (2018).
17. J. J. Giner-Sanz, E. M. Ortega, and V. Pérez-Herranz, "Montecarlo based quantitative Kramers–Kronig test for PEMFC impedance spectrum validation," Int. J. Hydrogen Energy **40**(34), 11279–11293 (2015).
18. K. Wang, Y. Wei, M. Zhao, *et al.*, "140-Gb/s PS-256-QAM Transmission in an OFDM System Using Kramers–Kronig Detection," IEEE Photonics Technol. Lett. **31**(17), 1405–1408 (2019).

19. A. J. Lowery and T. Feleppa, "Analog Low-Latency Kramers-Kronig optical Single-Sideband Receiver," J. Lightwave Technol. **39**(10), 3130–3136 (2021).
20. W.-R. Peng, B. Zhang, K.-M. Feng, *et al.*, "Spectrally Efficient Direct-Detected OFDM Transmission Incorporating a Tunable Frequency Gap and an Iterative Detection Techniques," J. Lightwave Technol. **27**(24), 5723–5735 (2009).
21. K. Zou, Y. Zhu, F. Zhang, *et al.*, "Spectrally efficient terabit optical transmission with Nyquist 64-QAM half-cycle subcarrier modulation and direct detection," Opt. Lett. **41**(12), 2767–2770 (2016).
22. Y. Chen and Y. Chen, "Simultaneous ICI and SSBI suppression in microwave photonic SEFDM transmission links using an iterative algorithm with random displacement of constellations," Opt. Laser Technol. **175**, 110767 (2024).